HEFAT2014
10th International Conference on Heat Transfer, Fluid Mechanics and Thermodynamics
14 – 16 July 2014
Orlando, Florida

# AN INTEGRATED ANALYTICAL APPROACH FOR SYSTEM-LEVEL TRANSIENT MODELING OF PASSIVE COOLING SYSTEMS

Gholami A., Ahmadi M., Bahrami M.*
*Author for correspondence
Laboratory for Alternative Energy Conversion (LAEC)
School of Mechatronic Systems Engineering
Simon Fraser University, Surrey, BC, Canada, V3T 0A3
E-mail: mbahrami@sfu.ca

## ABSTRACT

A new one-dimensional thermal network modeling approach is proposed that can accurately predict transient/dynamic temperature distribution of passive cooling systems. The present model has applications in variety of electronic, power electronic, photonics and telecom systems, especially where the system load fluctuates over time. The main components of a cooling system including: heat spreaders, heat pipes, and heat sinks as well as thermal boundary conditions such as natural convection and radiation heat transfer are analyzed, analytically modeled and presented in the form of resistance and capacitance (RC) network blocks. The present model is capable of predicting the transient/dynamic (and steady state) thermal behavior of cooling system with significantly less cost of modeling compared to conventional numerical simulations. Furthermore, the present method takes into account system 'thermal inertia' and is capable of capturing thermal lags in various components. The model is presented in two forms: 0-dimensional and 1-dimensional which are different in terms of complicacy. A custom-designed test-bed is also built and a comprehensive experimental study is conducted to validate the proposed model. The experimental results show great agreement, less than 4.5% relative difference in comparison with the modeling results.

## INTRODUCTION

The continued growth in performance and functionality of telecom, microelectronic, and photonics systems combined with miniaturization trend in the industry have resulted in a significant increase in heat generation rates [1–3], and presents a great challenge to thermal engineers. A number of failure mechanisms in electronic devices such as inter-metallic growth, metal migration, and void formation are directly linked to thermal effects. According to Arrhenius law, the rate of these failures is approximately doubled with every 10°C increase in the operating temperature of the device. In fact, more than 65% of system failures have thermal roots [4]. In addition, the fluctuations in the system loads can adversely impact the efficiency and reliability by forming temporary hotspots, thus thermal stresses. In optoelectronics, photonics and microelectronics, the ability to understand, predict and possibly minimize the thermal stresses such as brittle fracture, thermal fatigue, thermal shock and stress corrosion is of crucial importance [5], [6]. Electronics and telecommunication devices mainly operate in transient or pulsed mode, mainly in applications such as: AC/DC rectifiers, uninterruptible power supply (UPS) modules, Inverters and etc.

Among different cooling techniques, passive cooling methods are widely preferred since they provide low-cost, no-parasitic power, quiet operation and reliable cooling solutions. One method to model transient thermal systems is using thermal resistance-capacitance (RC) networks analog to electrical circuits [7]. In this analogy, voltage and current stand for temperature and heat flow rate, respectively. Such RC network models range from simple ones which only consider the most important thermal phenomena to complicated networks which include the details of the cooling system.

Steady state thermal resistance network models have been extensively studied in the literature, see e.g.[8–14]. There are also a few studies that include the capacitive behaviour of the components to account for transient heat transfer. Barcella *et al.* [15] presented a resistance-capacitance (RC) modeling method for architecture-level simulation of Very-Large-Scale-Integration (VLSI) chips. Following Barcella's work, Stan *et al.* [16] introduced a thermal RC modeling approach applicable to microprocessor dies and the attached heat sink. Magnone *et al.* and Cova *et al.* [17], [18] presented Cauer RC network model for transient conduction inside silicon power devices and power device assemblies. A thermal RC network model was introduced by Lopez-Walle *et al.* [19] that was capable of modeling heat transfer in micro thermal actuators for both static and dynamic modes. The RC network modeling concept also has been used in transient modeling of building solar gain [20–22]. The above studies are mostly limited to single component models with no analysis of thermal inertia and dynamic loadings effect. Also there is no general comprehensive and robust transient thermal network (RC) model for multi-component systems. In this study a new compact thermal network model is proposed that can accurately predict transient

and steady-state behaviour of electronic, power electronic and photonic systems.

The present RC thermal model is capable of covering the entire range of cooling solutions from module/component-level to system-level. To apply the thermal RC model to a system, first, all the components should be modeled individually by resistances and capacitances (R and C). Then, based on the heat flow, an equivalent thermal circuit should be formed using these RC blocks. One major advantage of the proposed thermal network method is its simplicity, i.e., the transient behaviour of the system under various operating and load conditions can be simulated rather easily without using complicated and time consuming numerical solutions.

The proposed RC model is focused on passive cooling systems; however, the same approach can be used for active cooling systems. The considered passive system includes heat spreader, heat pipe and naturally-cooled heat sink. The model is developed at two complicacy levels of 0-D and 1-D which support both transient and steady state conditions. The proposed model is capable of simulating any arbitrary loading and operating scenarios. A custom-designed test-bed is developed and several passive cooling systems are built and tested. The model is successfully validated with experimental data and an excellent agreement between the modeling results and experimental data is observed.

## NOMENCLATURE

| | | |
|---|---|---|
| $A, B$ | [-] | Temperature solution coefficients |
| $A_{source/sink}$ | [m$^2$] | Sources or sinks area |
| $C$ | [J/K] | Capacitance |
| $F$ | [-] | View factor |
| $L$ | [m] | Length (m) |
| $L_e$, $L_c$ | [m] | Heat pipe evaporator and condenser length (m) |
| $Q$ | [W] | Heat flow (W) |
| $R$ | [K/W] | Resistance (K/W) |
| $Ra$ | [-] | Rayleigh number |
| $T$ | [K] | Temperature (K) |
| $V_i$ | [m$^3$] | Volume of component I (m3) |
| $W$ | [m] | Width (m) |
| $X_i$, $Y_i$ | [m] | Source/sink center coordinates (m) |
| $a_i$, $b_i$ | [m] | Source or sink's length and width (m) |
| $c_i$ | [L/kg.K] | Specific heat capacity of component I (J/kg.K) |
| $g$ | [m/s$^2$] | gravity (m/s2) |
| $h$ | [W/m$^2$.K] | Convective heat transfer coefficient (W/m2.K) |
| $k$ | [W/m.K] | Thermal conductivity (W/m.K) |
| $m$, $n$ | [-] | Number of eigenvalues |
| $m_i$ | [kg] | Mass of component I (kg) |
| $n_f$ | [-] | Number of heat sink fins |
| $p$ | [m] | Fin depth (m) |
| $q$ | [W/m$^2$] | Heat flux (W/m2) |
| $r$ | [m] | Radius (m) |
| $s$ | [m] | Fin spacing (m) |
| $s_{ij}$ | [-] | Auxiliary coefficients of temperature solution |
| $\theta$ | [-] | Dimensionless temperature |
| $\alpha$ | [m$^2$/s] | Thermal diffusivity (m2/s) |
| $\beta$ | [1/K] | Thermal expansion coefficient (1/K) |
| $\varepsilon$ | [-] | Width to length ratio of plate |
| $\varepsilon_H$ | [-] | Height to length ratio of plate |
| $\varepsilon_i$ | [-] | Emissivity of surface i |
| $\kappa_x$, $\kappa_y$ | [-] | In-plane to through-plane thermal conductivity ratio in x and y directions |
| $\lambda, \delta, \beta$ | [-] | Temperature solution eigenvalues |
| $\sigma$ | [W/m$^2$.K$^4$] | Stefan-Boltzmann constant (W/m2.K4) |
| $\nu$ | [m$^2$/s] | Kinematic viscosity (m2/s) |

## MODEL DEVELOPMENT

In general, a passive multi-component cooling system includes the following main components: i) heat spreaders; ii) heat pipes; and iii) heat sinks. A schematic of a typical passive cooling system is shown in Fig. 1.

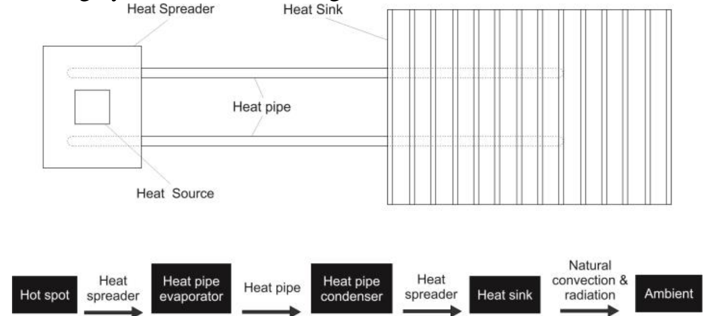


**Figure 1**. Left: Schematic and block diagram of a typical passive cooling system; Right: a modeled passive system test-bed.

Every component on the heat transfer path causes a temperature drop, i.e., resistance to the heat flow. This temperature drop is a function of geometry (dimensions and shape), thermo-physical properties of the component as well as the heat flow rate. The ratio of temperature drop over the rate of heat flow is known as thermal resistance [7].

$$R = \frac{\Delta T}{\dot{Q}} \quad (1)$$

where $\Delta T$ is temperature drop and $\dot{Q}$ is the heat transfer rate. System components also have thermal inertia acting as thermal capacitors that store or release heat during transient operation. This capacitive characteristic results in a "thermal lag" in the system response to variations, e.g. boundary conditions or thermal load. In addition to the components, there are also some thermal phenomena at the system boundaries and components' interface, such as natural convection, radiation and thermal contact resistance which should be considered as resistances against the heat flow. It should be noted, no capacitor have to be considered for the boundary phenomena as they do not show any thermal mass effect.

Knowing thermal resistances and capacitances, an RC model can be constructed and analyzed rather simply using software such as MATLAB, LTspice or SapWin, which enables simulation and accurate prediction of the thermal behaviour of any cooling system over time at each desired point in the system under any arbitrary operating scenario. To calculate the resistances and capacitances in an RC model, all the dimensions and thermal properties of the components as well as boundary conditions (e.g. ambient temperature) should be known. For the radiation thermal resistance, emissivity of the radiant surface should be known as well.

In the following sections two general network models are presented to predict the behaviour of thermal systems under both transient and steady state conditions. The first one which is called one-dimensional (1-D) model is more comprehensive, accurate and accommodates more details whereas the second model which is referred to as zero-dimensional (0-D) and is a simplified version of the 1-D model, is less accurate but faster.

Contact resistance due to comparatively small value is neglected in both models; however, it can be included in systems where contact resistance is important.

**1-D thermal network model**

Here, the thermal network model of a typical passive cooling system, shown in Fig. 1, is studied. The present model can be extended to any other passive (or active) cooling system with any number of components. The proposed 1-D RC model, for the system shown in Fig. 1, is demonstrated in Fig. 2.

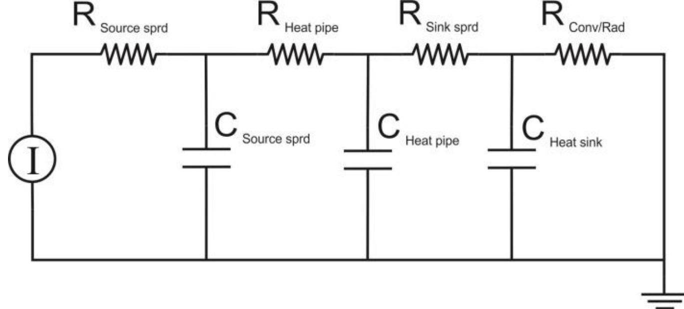


**Figure 2.** 1-D RC model of the passive cooling system shown in Fig. 1including: heat source, heat spreader at the heat source, heat pipe and naturally cooled heat sink

The capacitance of each component can be calculated using Eq. (2) which is the summation of all sub-components' capacities.

$$C = \sum_n m_n c_n = \sum_n \rho_n c_n V_n \tag{2}$$

where $m$ is the mass of each part, $c$ is the thermal capacity and $\rho$ and $V$ are the density and the volume of each part, respectively. However, the approach to define the resistance of each component is different. In the following section, a resistance model for each component is developed.

**1. Heat spreader resistance**

Most of heat spreaders are rectangular in shape with rectangular hot/cold spots on the top and bottom surfaces. We recently developed a new comprehensive analytically modeled for determining temperature distribution and thermal resistance of anisotropic heat spreaders [23]. Figure 3.a shows a schematic of a rectangular heat spreader with multiple hot/cold spots on its faces. The dimensions and the location of heat sources are depicted in Fig. 3.b.

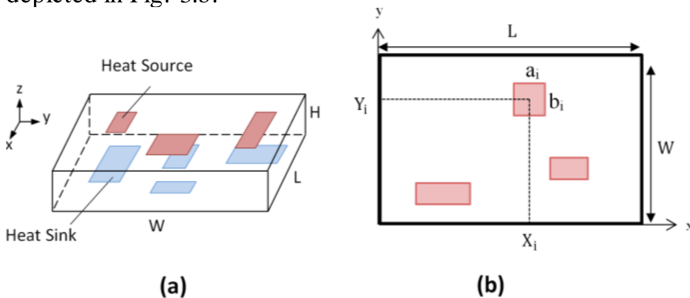


**Figure 3.** Schematic of a rectangular spreader with multiple hotspots on the top and bottom surfaces (a) Size and location of the hotspots (b)

The thermal resistance of such plates is defined as follows,

$$R = \frac{\dfrac{1}{A_{sources}} \displaystyle\sum_{Sources} \int_{Y_i - \frac{b_i}{2}}^{Y_i + \frac{b_i}{2}} \int_{X_i - \frac{a_i}{2}}^{X_i + \frac{a_i}{2}} T_{Sources}\, dxdy - \dfrac{1}{A_{Sinks}} \displaystyle\sum_{Sinks} \int_{Y_i - \frac{b_i}{2}}^{Y_i + \frac{b_i}{2}} \int_{X_i - \frac{a_i}{2}}^{X_i + \frac{a_i}{2}} T_{Sinks}\, dxdy}{\left| \displaystyle\iint_{Sources/Sinks} q_i\, dxdy \right|} \tag{3}$$

In order to calculate the average temperatures in Eq. (3), temperature distribution inside the heat spreader is needed. We developed an analytical solution for temperature distribution inside anisotropic heat spreaders with arbitrary heat flux on the hotspots and validated with experimental data in a different study [23]. The final results are presented in appendix A; more detail can be found in [23].

For irregular and non-rectangular heat spreaders, one may approximate the heat spreader geometry with the equivalent rectangular block to estimate the spreading resistance. One such example is the rectangular heat spreader used in the experimental test setup of this study which sandwiches one heat pipe and one cylindrical heater, Fig. 4.a. We approximated this heat spreader with two separate plates which are thermally connected in parallel. The hotspots are the projected areas of the cylinders, heat pipe and heater, on the surface, Fig. 4.b. with this approximation the equivalent resistance network of the spreaders will be two identical single plate resistances working in parallel; see Fig. 4.c, which can be readily calculated using Eq. (10).

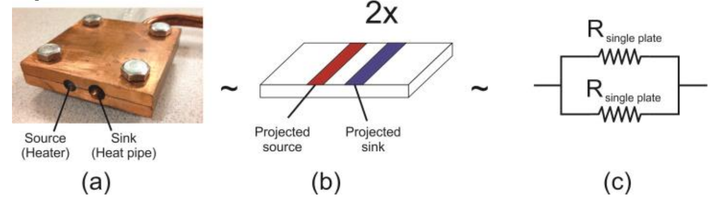


**Figure 4.** Heat spreaders of the present experimental test setup, sandwiching one heat pipe and one cylindrical electric heater (a) real geometry (b) approximated heat spreader geometry, and (c) equivalent thermal resistance network model.

**2. Heat pipe resistance**

In a heat pipe, heat is transported through three paths: i) inner hollow, through conduction and convection, ii) wick, through conduction, iii) wall, through conduction. Figure 5 shows the thermal resistance circuit of a heat pipe.

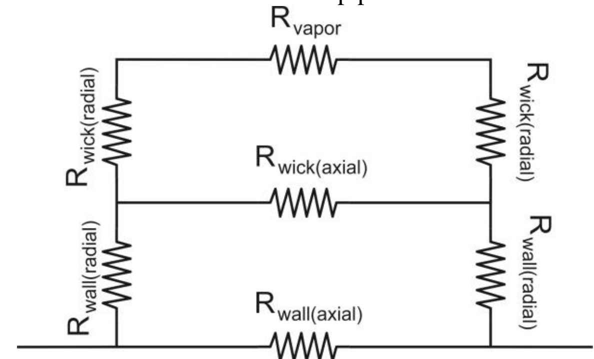


**Figure 5.** Thermal resistance network model of heat pipe (steady state)

In Fig. 5, the axial resistances have comparatively large values, so they can be assumed as open circuit. On the other hand, the vapor resistance is very small and can be assumed as short circuit [13][24][25].

Applying these simplifications and considering the thermal storage of a heat pipe, thermal network of a heat pipe can be represented as shown in Fig. 6.

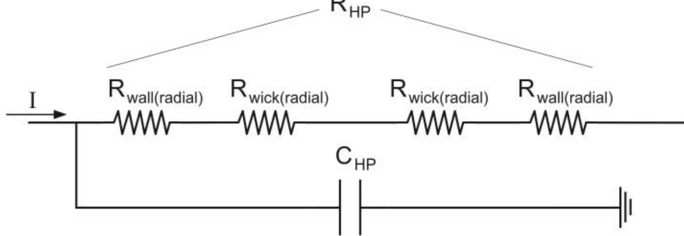


**Figure 6.** Simplified thermal network model of heat pipe

The radial thermal resistance for a cylinder wall with inner and outer radiuses of $r_1$ and $r_2$ and length of $L$ with thermal conductivity of $k$ is:

$$R_r = \frac{\ln\left(\frac{r_2}{r_1}\right)}{2\pi kL} \tag{4}$$

Thus, the resistance of a cylindrical heat pipe is simply the summation of all the resistances shown in Fig. 6:

$$R_{HP} = \frac{L_e + L_c}{2\pi L_e L_c}\left(\frac{\ln\left(\frac{r_{out}}{r_{wall}}\right)}{k_{wall}} + \frac{\ln\left(\frac{r_{wall}}{r_{wick}}\right)}{k_{wick}}\right) \tag{5}$$

where $r_{out}$ is the pipe outer radius, $r_{wall}$and $r_{wick}$ are inner radii of the wall and the wick, $L_e$ and $L_c$ are the length of the evaporator and the condenser sections, and $k_{wall}$ and $k_{wick}$ are thermal conductivities of the wall and effective thermal conductivity of the wick, respectively. The capacitance of the heat pipe is calculated using Eq. (2).

### 3. Heat sink spreading resistance

To use the present 1-D model, we should assume a uniform temperature for heat sinks. This assumption is not far from reality for most engineering applications, however; it may introduce some inaccuracy in the model. As the heat enters from the heat sink base to be transferred to the surroundings, it encounters a spreading resistance in the base, which causes a temperature drop inside the heat sink. Uniform temperature assumption on the outer surface implies that the fins thermal resistance is negligible compared to the base plate resistance. Neglecting the resistance of the fins simplifies the heat sink's thermal resistance into the resistance of a rectangular block whose thickness is equal to the thickness of the base plate. In this block heat sources are the projected area of the hotspots on the back face, and heat sinks are a series of alternate rectangular strips with length of the block width, and widths of fin thickness and fin spacing which cover the whole surface of block, as shown in Fig 7. Assuming a uniform convective heat transfer coefficient over the heat sink surface, the dissipated heat through the strips on the equivalent block can be determined using its corresponding area in the real heat sink. For a heat sink with $n_f$ fins, fin spacing of $s$, fin thickness of $t$ and fin depth of $p$, the heat transfer will be,

$$Q_{fin} = \frac{2p+t}{2n_f p + L} Q_{in}$$
$$Q_{base} = \frac{s}{2n_f p + L} Q_{in} \tag{6}$$

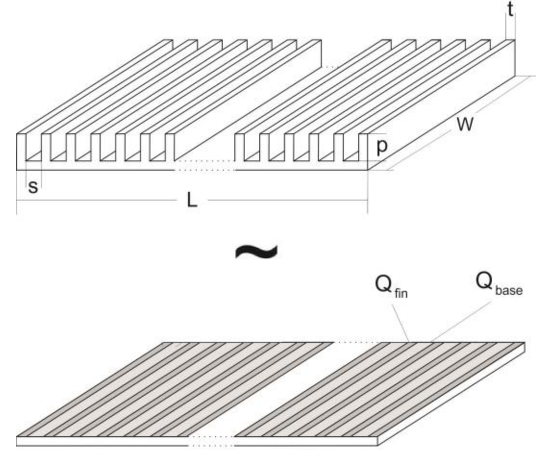


**Figure 7.** Rectangular finned heat sink and its base rectangular shape equivalent spreader

Having the heat sink simplified to the above-mentioned geometry which is a multi-hotspot rectangular heat spreader, the spreading resistance can be calculated using the approach explained in section 2.2.1.

### 4. Convective/radiative resistance

On the surface of a heat sink, heat is dissipated to the ambient through two parallel mechanisms: i) natural convection and ii) radiation [26]. Using the definition of the thermal resistance, Eq. (1), the thermal resistance of a heat sink can be defined as,

$$R = \frac{\Delta T}{Q_{convection} + Q_{Radiation}} \tag{7}$$

where $\Delta T$ is the temperature difference between the surface of the heat sink and the ambient. The amount of convective heat transfer is the summation of heat transfers from the fins and the base,

$$Q_{Convection} = h_f A_f \Delta T + h_b A_b \Delta T \tag{8}$$

where the subscripts $f$ and $b$ refer to 'fin' and 'base plate', respectively.

The following correlations are used for calculating the convective heat transfer coefficient in rectangular finned heat sinks [26],

$$h_b = \frac{k}{L} 0.59 Ra_L^{0.25} \quad \text{Single plate (base plate)} \tag{9}$$

$$h_f = \frac{k}{s}\left[\frac{576}{\left(\frac{Ra_s s}{L}\right)^2} + \frac{2.873}{\left(\frac{Ra_s s}{L}\right)^{0.5}}\right]^{-0.5} \quad \text{Parallel plates (fins)} \tag{10}$$

where

$$Ra_x = \frac{g\beta}{\vartheta\alpha}(T_s - T_{amb})x^3 \tag{11}$$

In the above correlations, $L$ and $s$ are fin length and fin spacing of the heat sink, respectively. Other types of heat sinks can be modeled using a similar approach.

For radiation heat transfer, the following correlation is used [26],

$$Q_{Radiation} = \sigma\left(T_s^4 - T_{amb}^4\right)\left(\sum_i \frac{1}{\frac{1-\varepsilon_i}{A_i\varepsilon_i} + \frac{1}{A_i F_{i\infty}}}\right) \tag{12}$$

where $\sigma$, $\varepsilon$ and $F$ are Stefan-Boltzmann coefficient, emissivity and the view factor of surface $i$, respectively. The view factor of a single duct surface of heat sink for comparatively small fin aspect ratios can be calculated using the following approximation,

$$F = \frac{s}{s+2p} \tag{13}$$

Substituting the correlations for both convective and radiative heat transfers, Eqs. (8) and (12), into the resistance definition, Eq. (1), the following relationship for the thermal resistance of a rectangular heat sink is derived,

$$R = \frac{1}{h_f A_f + h_b A_b + \sigma\left(T_s^2 + T_{amb}^2\right)(T_s + T_{amb})\left(\sum_i \frac{1}{\frac{1-\varepsilon_i}{A_i\varepsilon_i} + \frac{1}{A_i F_{i\infty}}}\right)} \tag{14}$$

Equation (14) shows that the resistance is a function of thermo-physical properties as well as the temperature of both heat sink and the environment.

**0-D thermal network model**

This model is a simplified form of the above 1-D model in which all the comparably small resistances in the system, shown in Fig. 1, are neglected.

The convective and radiative thermal resistances on the heat sink, which are an order of magnitude larger than the others, are the only resistances considered. Applying the above mentioned simplifications, the equivalent RC model of the system shown in Fig. 1 is shown in Fig. 8.

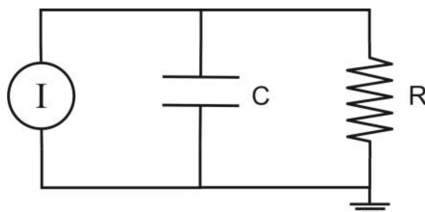


**Figure 8.** A 0-D RC network model of the passive cooling system shown in Fig. 1

In Fig. 8, the resistance is calculated according to section 2.1.4 and the capacitance is the summation of the capacity of all the components of the system, calculated using Eq. (2).

## EXPERIMENTAL STUDY

To validate the present model, a custom-designed experimental test setup is built. The test setup is a passive cooling mechanism consisting of two electric cartridge heaters with the maximum rated powers of 40W supplied by OMEGA (Toronto, ON), and are connected to a naturally-cooled rectangular finned heat sink via round heat pipes (Fig 10). The middle section of heat pipes were insulated in the final setup. Heaters are sandwiched between copper plates which work as heat spreaders. The heaters are powered by an adjustable AC power supply (VARIAC, China). To monitor and log the temperature data, T-type thermocouples with uncertainty of ±0.5°C in conjunction with National Instrument (NI) DAQ system are used. Thermocouples are fully attached to the surface using thermal paste. Dimensions and thermal properties of the test-bed components are listed in Table 1.

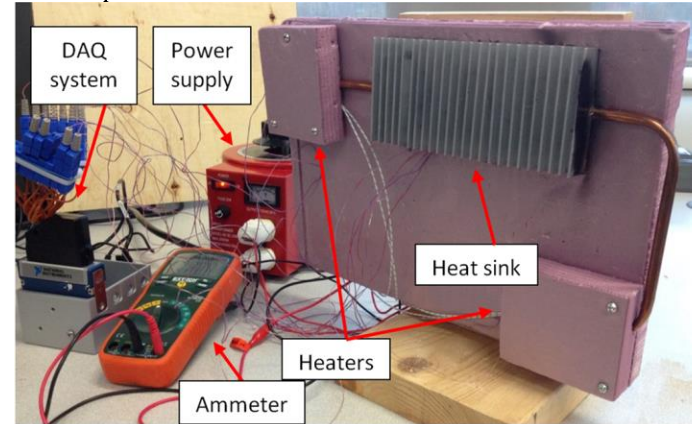


(a)

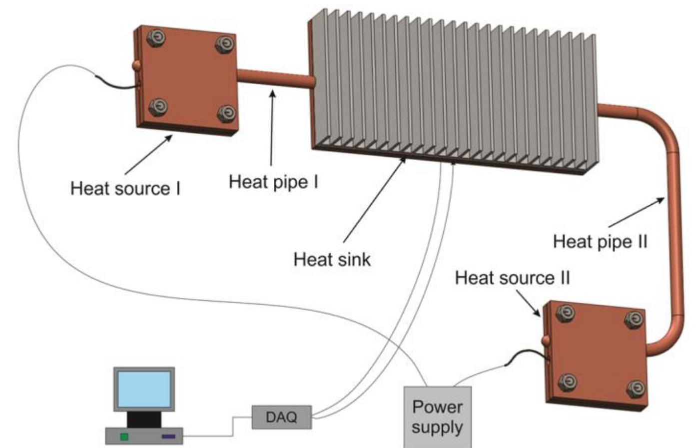


(b)

**Figure 9.** (a) test-bed and (b) schematic of the two-path experimental test-bed

Table 1 Test-bed thermo-physical specifications

| | Spreader I | Spreader II | Heat pipe I & II | Heat sink |
|---|---|---|---|---|
| Material | Copper | Copper | Copper | Aluminum |
| Length [mm] | 63 | 63 | $L_{HP-I}$= 300<br>$L_{HP-II}$= 200<br>$L_e$ = 30<br>$L_c$ = 30 | 185 |
| Width [mm] | 63 | 63 | -- | 86 |
| Thickness [mm] | 6 | 6 | $t_{wall}$= 0.8<br>$t_{wick}$ = 1.2 | $t_{base}$ = 5<br>$t_{fin}$ = 2 |
| Diameter [mm] | -- | -- | $D_{out}$ = 8 | -- |
| Fin depth [mm] | -- | -- | -- | 17 |
| Fin spacing [mm] | -- | -- | -- | 6 |
| Thermal conductivity [W/m.K] | 400 | 400 | $k_{Copper}$ = 400<br>$k_{wick}$ = 50 | 120 |
| Density [kg/m$^3$] | 8960 | 8960 | 8960 | 2700 |
| Specific heat [J/kg.K] | 386 | 386 | 386 | 900 |

**Test procedure**

Different step and oscillatory loading scenarios are imposed to the cooling system by heaters and the temperature data is monitored and logged throughout the experiment. Each test is carried out for the transition time starting from the initial equilibrium state in which all the components are in equilibrium with the ambient, to the final steady state. At the steady state, the temperature becomes either statically or "dynamically" steady depending on the load profile of the heaters. For temperature measurement, 16 thermocouples are attached to different locations in the test-bed to keep track of temperature variations at important locations. To investigate the thermal behavior of the system in different load cycles and validate the present 0-D and 1-D models, the experiments are conducted for the following two different loading scenarios:

I. Static loading; each heater has a constant power.
II. Dynamic loading; each heater has a cyclic heat load profile.

Applying the methodology described earlier, the present 1-D RC model of the test-bed is shown in Fig. 10. For the 0-D RC model, the RC network has the form shown in Fig 8. The values of the components are listed in Table 2.

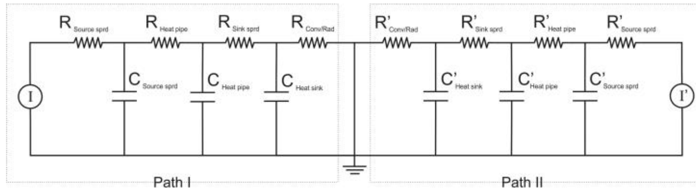


**Figure 10.** 1-D model of the two-path experimental test-bed

Table 2: Component values of the 1-D RC model of the two-path experimental test setup

| | Resistance [K/W]/ Capacitance [J/K] | | | |
|---|---|---|---|---|
| | Heat source Spreader | Heat pipe | Heat sink spreader | Convection & radiation |
| 1-D (path I) | 0.052/140 | 0.014/18 | 0.19/350 | 1.5/- |
| 1-D (path II) | 0.052/140 | 0.014/27 | 0.19/350 | 1.5/- |
| 0-D | $R_{total}$ =1.5/1025 | | | |

**Model validation**

To validate the proposed models, experimental data recorded for different heating scenarios are plotted and compared with their corresponding model simulations. Three important locations, two on the heat sources and one on the heat sink, are chosen as benchmarks for comparison and validation. In Fig. 11 the temperature at these three spots are compared with the 1-D as well as the 0-D model for the static loading of 10 watts for heater I and 14 watts for heater II.

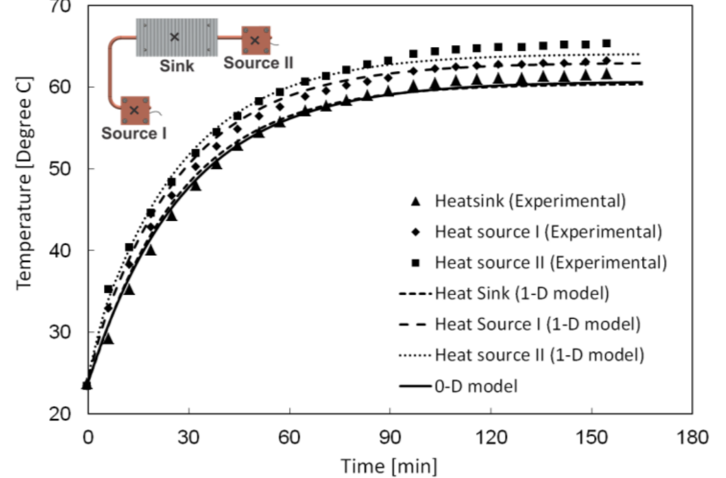


**Figure 11.** 0-D model validation with experimental data at three locations of heat sink and two heat sources for the heating scenario of constant 14W for heater I and 10W for heater II

As the 0-D model only provides one temperature for the whole test-bed as a lumped mass, it is not capable to detect the temperature difference between the heat sinks and heat sources. Therefore, in Fig. 11, it can be seen that the 0-D model captures the heat sink temperature reasonably well with less than 2% relative difference. However; it is not capable of predicting other components temperature such as heat sources. The present 1-D model however is capable of accurately predicting temperatures at different spots as it considers the thermal resistance between the components. The maximum relative difference with the experimental data with the 1-D model is approximately 4%. Figure 12 depicts another static loading case (Heater I, 5W and heater II, 9W) in which again the heat sink temperature is accurately predicted by both 0-D and 1-D model

whereas the temperature of the heat sources can only be predicted by the 1-D model.

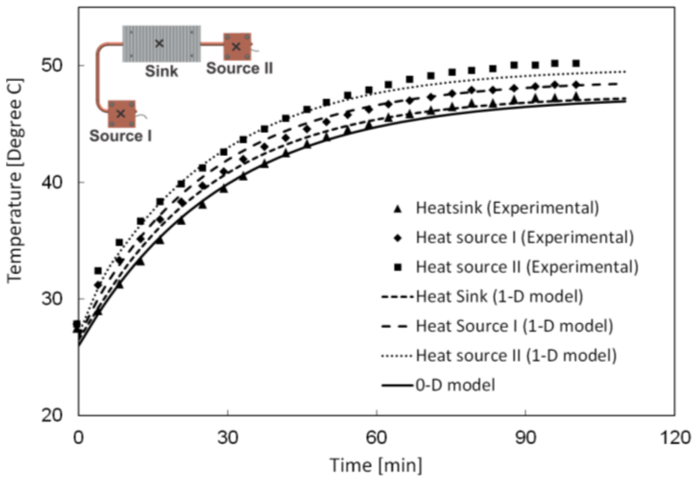


**Figure 12.** 0-D model validation with experimental data at three locations of heat sink and two heat sources for the heating scenario of constant 9W for heater I and 5W for heater II

Figures 11 and 12 indicate that the temperature of other locations in the test-bed has almost the same trend as the temperature of the heat sink with a small offset. It can be interpreted that for cases with no sharp variation in heat source power, the 0-D model is sufficient if the purpose is only to predict an estimation of the system temperature. Obviously, for variable loading situations in which the internal thermal resistances and thermal inertia become important, a 0-D model cannot provide detailed information.

The following two dynamic loading scenarios are selected arbitrarily: i) heater I with a constant heat generation of 13W and heater II with a pulsating heat generation with a maximum of 20W and a minimum of 0 and the period of 20 minutes; and ii) heater I with a two-step pulsating heat generation with the profile shown in Fig. 15 and heater II turned off.

Figure 13 presents the measured temperatures over time at three specified spots as well as the both models results for heat sink temperature. Both 0-D and 1-D models have predicted the heat sink temperature accurately. As it is seen, unlike the static form of loading, the shape of temperature variation for dynamic loading is different at various locations. These differences are due to thermal inertia effects and the 0-D model is unable to detect them. The 1-D model results for the two heat sources are shown in Fig. 14. It is indicated that the 1-D model performs very good and captures the trend of the temperature fluctuation at the two hotspots. The relative difference between the model and experimental data in this case is less than 4%.

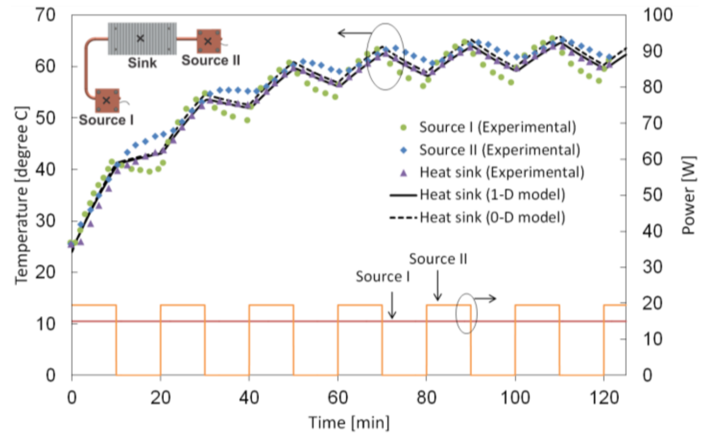


**Figure 13.** Comparison of 0-D model with experimental temperature of three different locations on the test bed for the applied dynamic loading of shown in the figure

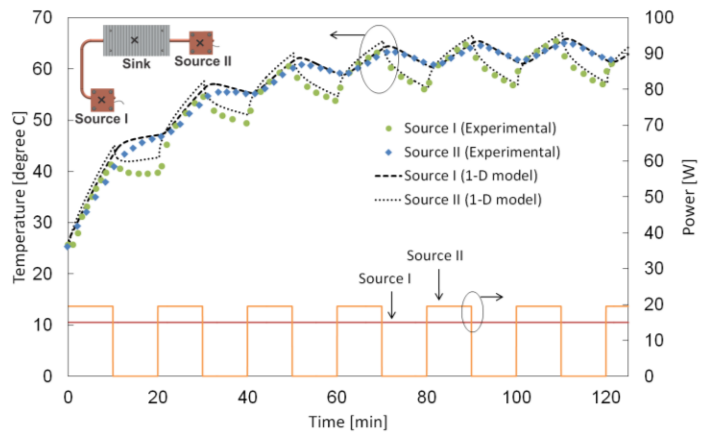


**Figure 14.** 1-D model validation with experimental data at two heat source locations for the imposed dynamic loading shown

The comparison for the second scenario is shown in Figs. 15 and 16. This loading scheme represents the worst case in terms of fluctuation and thermal inertia effect on the thermal behavior of the system. As it is seen in Fig. 15, both models capture the heat sink temperature very well. It is worth noting that the temperature variation at the pulsating heater is very sharp while at the other heat source the temperature fluctuates much smoother with a lag in responding to the power changes, which is due to the damping effect caused by thermal inertia of the system components. This effect is completely captured by the 1-D model and the results for these two temperatures are plotted and compared with our experimental data in Fig. 16. The maximum relative difference between the model and experimental data is approximately 4.5%.

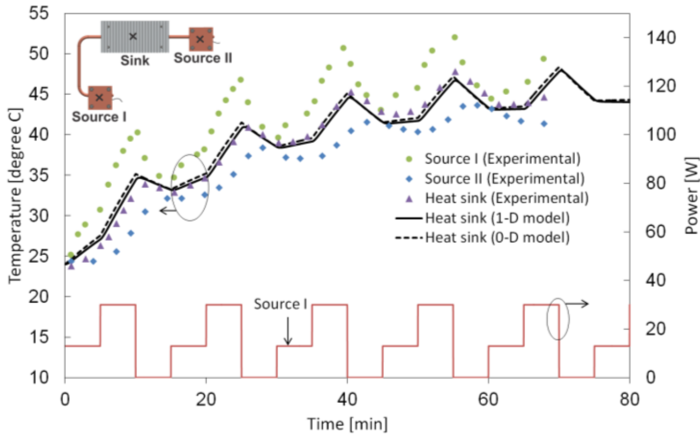


**Figure 15.** Comparison of 0-D model with experimental temperature of three different locations on the test bed for the imposed dynamic loading shown in the figure

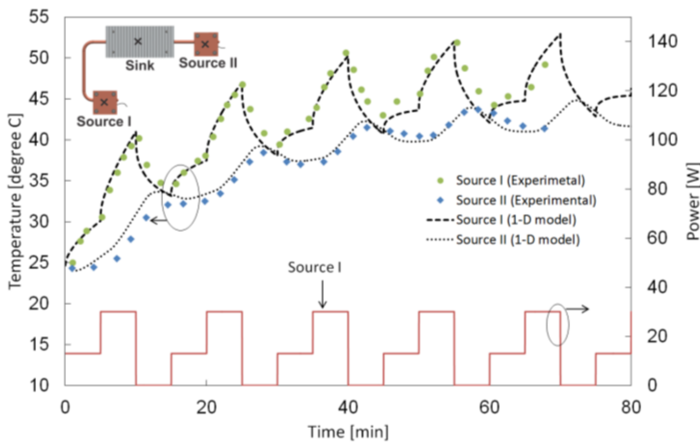


**Figure 16.** 1-D model validation with experimental data at two heat source locations for the imposed dynamic loading shown in the figure

## SUMMARY AND CONCLUSION

A new analytical methodology is developed that can accurately predict the dynamic thermal responses of electronic, power electronic, telecom cooling systems. The passive cooling solution components are modeled including: heat spreaders, heat pipes and heat sinks. The compartments are modeled individually with a network of resistances and capacitances which represents the transient thermal behavior of that compartment. Then the corresponding R and C blocks are appropriately assembled to form a network to represent the thermal system. Compact relationships are presented for the resistances and capacitance of the considered passive compartment. Convection and radiation heat transfer on the heat sink are also modeled as a resistance in the model. By analyzing the equivalent thermal circuit, the model is capable of predicting the temperature distribution of the system in both transient and steady state for any loading scenario. Two versions of the present RC model are proposed: i) 0-D that is much simpler but provides a rough estimate of system thermal behaviour; and ii) 1-D: a more complicated which provides more details. To validate the present RC model, a two-path passive cooling test-bed consisting of two heaters connected to a heat sink using two heat pipes and two spreaders is built. The test-bed is used for different dynamic thermal loading scenarios; and the temperatures at 16 locations are measured and recorded. The comparison between the proposed model and the experimental data shows an excellent agreement with relative difference of approximately 4.5%.

## REFERENCES


[1] S. P. Gurrum, S. Member, S. K. Suman, Y. K. Joshi, S. Member, and A. G. Fedorov, "Thermal Issues in Next-Generation Integrated Circuits," vol. 4, no. 4, pp. 709–714, 2004.

[2] R. J. McGlen, R. Jachuck, and S. Lin, "Integrated thermal management techniques for high power electronic devices," *Applied Thermal Engineering*, vol. 24, no. 8–9, pp. 1143–1156, Jun. 2004.

[3] Z. Zuo, L. R. Hoover, and A. L. Phillips, "Advanced thermal architecture for cooling of high power electronics," *IEEE Transactions on Components and Packaging Technologies*, vol. 25, no. 4, pp. 629–634, Dec. 2002.

[4] B. Wunderle and B. Michel, "Progress in reliability research in the micro and nano region," *Microelectronics Reliability*, vol. 46, no. 9–11, pp. 1685–1694, Sep. 2006.

[5] E. Suhir, "Thermal Stress Failures in Electronics and Photonics: Physics, Modeling, Prevention," *Journal of Thermal Stresses*, vol. 36, no. 6, pp. 537–563, Jun. 2013.

[6] E. Suhir, D. Shangguan, and L. Bechou, "Predicted Thermal Stresses in a Trimaterial Assembly With Application to Silicon-Based Photovoltaic Module," *Journal of Applied Mechanics*, vol. 80, no. 2, Jan. 2013.

[7] Y. Kakaç S., Yener, "ONE-DIMENSIONAL STEADY-STATE HEAT CONDUCTION," in *Heat Conduction*, 3rd ed., 1993.

[8] S. Moghaddam, M. Rada, a. Shooshtari, M. Ohadi, and Y. Joshi, "Evaluation of analytical models for thermal analysis and design of electronic packages," *Microelectronics Journal*, vol. 34, no. 3, pp. 223–230, Mar. 2003.

[9] X. Luo, Z. Mao, J. Liu, and S. Liu, "An analytical thermal resistance model for calculating mean die temperature of a typical BGA packaging," *Thermochimica Acta*, vol. 512, no. 1–2, pp. 208–216, Jan. 2011.

[10] S. Liu, B. Leung, A. Neckar, S. O. Memik, G. Memik, and N. Hardavellas, "Hardware/software techniques for DRAM thermal management," *2011 IEEE 17th International Symposium on High Performance Computer Architecture*, pp. 515–525, Feb. 2011.

[11] R. Zhao, L. Gosselin, M. Fafard, and D. P. Ziegler, "Heat transfer in upper part of electrolytic cells: Thermal circuit and sensitivity analysis," *Applied Thermal Engineering*, vol. 54, no. 1, pp. 212–225, May 2013.

[12] a. A. El-Nasr and S. M. El-Haggar, “Effective thermal conductivity of heat pipes,” *Heat and Mass Transfer*, vol. 32, no. 1–2, pp. 97–101, Nov. 1996.

[13] J. Zuo and A. Faghri, “A network thermodynamic analysis of the heat pipe,” *Int. J. Heat Mass Transfer*, vol. 41, no. 11, pp. 1473–1484, 1998.

[14] H. Shabgard and A. Faghri, “Performance characteristics of cylindrical heat pipes with multiple heat sources,” *Applied Thermal Engineering*, vol. 31, no. 16, pp. 3410–3419, Nov. 2011.

[15] M. Barcella, W. Huang, K. Skadron, and M. Stan, “Architecture-Level Compact Thermal R-C Modeling,” 2002.

[16] M. R. Stan, K. Skadron, M. Barcella, W. Huang, K. Sankaranarayanan, and S. Velusamy, “HotSpot: a dynamic compact thermal model at the processor-architecture level,” *Microelectronics Journal*, vol. 34, no. 12, pp. 1153–1165, Dec. 2003.

[17] P. Magnone, C. Fiegna, G. Greco, G. Bazzano, S. Rinaudo, and E. Sangiorgi, “Numerical simulation and modeling of thermal transient in silicon power devices,” *Solid-State Electronics*, vol. 88, pp. 69–72, Oct. 2013.

[18] P. Cova, M. Bernardoni, N. Delmonte, and R. Menozzi, “Dynamic electro-thermal modeling for power device assemblies,” *Microelectronics Reliability*, vol. 51, no. 9–11, pp. 1948–1953, Sep. 2011.

[19] B. López-Walle, M. Gauthier, and N. Chaillet, “Dynamic modelling for thermal micro-actuators using thermal networks,” *International Journal of Thermal Sciences*, vol. 49, no. 11, pp. 2108–2116, Nov. 2010.

[20] A. P. Ramallo-González, M. E. Eames, and D. a. Coley, “Lumped parameter models for building thermal modelling: An analytic approach to simplifying complex multi-layered constructions,” *Energy and Buildings*, vol. 60, pp. 174–184, May 2013.

[21] A. Buonomano and A. Palombo, “Building energy performance analysis by an in-house developed dynamic simulation code: An investigation for different case studies,” *Applied Energy*, vol. 113, pp. 788–807, Jan. 2014.

[22] A. Athienitis, “Modeling and Simulation of Passive and Active Solar Thermal Systems,” in *Comprehensive Renewable Energy*, vol. 3, Elsevier Ltd., 2012, pp. 357–418.

[23] A. Gholami and M. Bahrami, “Thermal Spreading Resistance in Anisotropic Rectangular Plates with Multiple Heat Sources and Sinks,” *10th International Conference on Heat Transfer, Fluid Mechanics and Thermodynamics(HEFAT)*, 2014.

[24] C. Ferrandi, F. Iorizzo, M. Mameli, S. Zinna, and M. Marengo, “Lumped parameter model of sintered heat pipe: Transient numerical analysis and validation,” *Applied Thermal Engineering*, vol. 50, no. 1, pp. 1280–1290, Jan. 2013.

[25] N. Zhu and K. Vafai, “Analysis of cylindrical heat pipes incorporating the e€ ffects of liquid-vapor coupling and non-Darcian transport-a closed form solution,” *International Journal of Heat and Mass Transfer*, vol. 42, pp. 3405–3418, 1999.

[26] F. Incropera, D. DeWitt, and T. Bergrnan, *Fundamentals of Heat and Mass Transfer (The 6th Edition)*, 6th ed. 2007.

# Appendix A

The following is the final solution for temperature distribution inside an anisotropic rectangular plate with multiple hot/cold spots on the top and bottom surfaces,

$$\theta = A_0 z^*$$
$$+\sum_{m=1}^{\infty}\cos\left(\lambda\kappa_x x^*\right)\times\left[A_m\cosh\left(\lambda z^*\right)+B_m\sinh\left(\lambda z^*\right)\right]$$
$$+\sum_{n=1}^{\infty}\cos\left(\delta\kappa_y y^*\right)\times\left[A_n\cosh\left(\delta z^*\right)+B_n\sinh\left(\delta z^*\right)\right]$$
$$+\sum_{n=1}^{\infty}\sum_{m=1}^{\infty}\cos\left(\lambda\kappa_x x^*\right)\cos\left(\delta\kappa_y y^*\right)\times\left[A_{mn}\cosh\left(\beta z^*\right)+B_{mn}\sinh\left(\beta z^*\right)\right]$$

Where $\lambda$, $\delta$ and $\beta$ are eigenvalues and $A$ and $B$ coefficients are defined in the form of below:

$$\lambda = \frac{m\pi}{\kappa_x}, \qquad \delta = \frac{n\pi}{\kappa_y\varepsilon}, \qquad \beta = \sqrt{\lambda^2+\delta^2}$$

$$A_0 = \frac{s_{00}^t}{\varepsilon} = \frac{s_{00}^b}{\varepsilon}$$

$$A_m = \frac{2}{\varepsilon\lambda}\left(s_{m0}^b\operatorname{csch}\left(\lambda\varepsilon_H\right) - s_{m0}^t\coth\left(\lambda\varepsilon_H\right)\right)$$

$$A_n = \frac{2}{\varepsilon\delta}\left(s_{0n}^b\operatorname{csch}\left(\delta\varepsilon_H\right) - s_{0n}^t\coth\left(\delta\varepsilon_H\right)\right)$$

$$A_{mn} = \frac{4}{\varepsilon\beta}\left(s_{mn}^b\operatorname{csch}\left(\beta\varepsilon_H\right) - s_{mn}^t\coth\left(\beta\varepsilon_H\right)\right)$$

$$B_m = \frac{2s_{m0}^t}{\varepsilon\lambda} \quad B_n = \frac{2s_{0n}^t}{\varepsilon\delta} \quad B_{mn} = \frac{4s_{mn}^t}{\varepsilon\beta}$$

In which the auxiliary coefficients ‘$s$’s are,

$$s_{00}^{t\,or\,b} = \iint_{t\,or\,b} q_{i(x,y)}^*\,dx^*dy^*$$

$$s_{m0}^{t\,or\,b} = \iint_{t\,or\,b} q_{i(x,y)}^*\times\cos\left(\lambda\kappa_x x^*\right)dx^*dy^*$$

$$s_{0n}^{t\,or\,b} = \iint_{t\,or\,b} q_{i(x,y)}^*\times\cos\left(\delta\kappa_y y^*\right)dy^*dx^*$$

$$s_{mn}^{t\,or\,b} = \iint_{t\,or\,b} q_{i(x,y)}^*\times\cos\left(\lambda\kappa_x x^*\right)\cos\left(\delta\kappa_y y^*\right)dx^*dy^*$$